On the kinetics and conformational dynamics of elevator transporters

Trinco, Gianluca

DOI:
10.33612/diss.177792564

Chapter 2

Kinetic mechanism of Na^+-coupled aspartate transport catalyzed by Glt_{Tk}

Gianluca Trinco[1], Valentina Arkhipova[1], Alisa A. Garaeva[1], Cedric A.J. Hutter[2], Markus A. Seeger[2], Albert Guskov[1,3] and Dirk J. Slotboom[1]

[1] Groningen Biomolecular Sciences and Biotechnology Institute, University of Groningen, Nijenborgh 4, 9747 AG, Groningen, The Netherlands
[2] Institute of Medical Microbiology, University of Zurich, Zurich, Switzerland
[3] Moscow Institute of Physics and Technology, Dolgoprudny, Russia

Abstract

It is well-established that the secondary active transporters Glt_{Tk} and Gl_{tPh} catalyse coupled uptake of aspartate and three sodium ions, but insight in the kinetic mechanism of transport is fragmentary. Here, we systematically measured aspartate uptake rates in proteoliposomes containing purified Glt_{Tk}, and derived the rate equation for a mechanism in which two sodium ions bind before and another one after aspartate. Re-analysis of existing data on Glt_{Ph} using this equation allowed for determination of the turnover number (0.14 s^{-1}), without the need for error-prone protein quantification. To overcome the complication that purified transporters may adopt right-side-out or inside-out membrane orientations upon reconstitution, thereby confounding the kinetic analysis, we employed a rapid method using synthetic nanobodies to inactivate one population. Oppositely oriented Glt_{Tk} proteins had undiscernible kinetic properties, consistent with the use of an identical gating element on both sides of the membrane. Our work, combined with previous pre-equilibrium binding studies, provides the most complete kinetic analysis of the structurally characterized aspartate transporters of the SLC1A family, and underlines the value of transport experiments to reveal mechanistic features of Na^+- aspartate symport that cannot be observed in detergent solution.

Introduction

Excitatory amino acid transporters (EAATs) of the solute carrier family 1A (SLC1A) take up the neurotransmitter L-glutamate from the synaptic environment, which is necessary to keep the extracellular concentration low and prevent neurotoxicity [1,2]. EAATs couple uptake of one amino acid substrate molecule to the co-transport of three sodium ions and one proton and counter-transport of one potassium ion [3–6]. Thus, glutamate gradients of a million-fold across the membrane under resting conditions can be sustained. The closely related archaeal transporters Glt_{Ph} from *Pyrococcus horikoshii* and Glt_{Tk} from *Thermococcus kodakarensis* of the SLC1A family (78% sequence identity to each other, ~36% sequence identity to EAATs) take up aspartate rather than glutamate in symport with three sodium ions, and are not coupled to potassium or proton transport [7–11]. These prokaryotic homologues of the neurotransmitter transporters have been instrumental in delineating shared structural features of this transporter family [7,8,19–22,9,12–18].

SLC1A family proteins are homotrimers, with independently operating protomers [19,21,23–29], each organized in two domains. A rigid scaffold domain mediates all the contacts with the neighbouring protomers, and a peripheral transport domain binds the amino acid substrate and cations [13,16,30,31]. The transport domains are mobile and move through the lipid bilayer (alike an elevator) when translocating the amino acid substrate and co-transported ions across the membrane [13]. During movement of the transport domain, the substrate binding site is occluded from the solvent and shielded by the tips of two pseudo-symmetrical helical hairpins (HP1 and HP2). The latter hairpin is a gating element that can hinge between a closed position (taken during elevator movements) and an open position (allowing loading or release of substrate and co-transported ions). The extent of the elevator-like movement of the transport domain is so large (~20 Å in Glt_{Tk}) that HP2 acts as gating element both on the extracellular and the intracellular side of the membrane.

Transport assays in proteoliposomes have revealed that both Glt_{Ph} and Glt_{Tk} catalyse electrogenic transport with a strict stoichiometry of three co-transported Na^+ ions per aspartate [14,32]. Data from studies on equilibrium binding and pre-equilibrium kinetics of binding with the solubilized proteins in detergent solution have shown that co-transported ions and aspartate bind in a highly cooperative way, which is crucial to ensure thermodynamic coupling [10,15,33–37]. These experiments have indicated that most likely two sodium

ions bind first, then aspartate, and finally the third sodium ion. Binding of the last Na^+ leads to gate closure of HP2, which in turn is a prerequisite for elevator-like conformational changes that translocate the bound cargo across the membrane. Structures of Glt_{Ph} and Glt_{Tk} have provided a qualitative explanation for the observed binding order. Two of the sodium binding sites (named Na1 and Na3) are buried deep in the proteins [15]. A substantial conformation rearrangement in the apo-protein (most pronounced in the conserved unwound region of TM7) is required to create the geometry needed for sodium binding, which makes this step slow. The conformational rearrangement, which is stabilized by binding of the two sodium ions, also affects residues involved in aspartate binding. While the apo state does not have measurable affinity for aspartate, sodium binding creates a high-affinity site for amino acid substrate. The last sodium ion binds to a site in a direct contact with HP2 gate (Na2), and locks the gate in the closed position, with aspartate and the three sodium ions occluded from the environment.

Despite the enormous amount of data on structure and binding mechanism in detergent solution, insight in the kinetic mechanism under translocating conditions is fragmented and incomplete. Here, we set out to determine the kinetic mechanism of aspartate transport by using purified Glt_{Tk}, reconstituted in proteoliposomes. We measured initial rates of transport at a wide range of substrate and co-ion concentrations, a method that has been used extensively for the mechanistic characterization of enzymes, leading to insight in the order of binding of substrates [38]. This method has not been used much on purified membrane transporters, in part because it is often impossible to control the orientation of the reconstituted transporters in proteoliposomes, leading to mixed populations, thus complicating kinetic analysis.

To overcome this latter problem, we isolated an inhibitory synthetic nanobody [39], which we used to inactivate membrane transporters oriented in one of the two possible orientations. This method is rapid, generally applicable, and does not depend on mutagenesis and chemical modifications. The work presented here, combined with the results of previous pre-equilibrium binding studies [36], allows for determination of accurate turnover numbers, which we illustrate by analysing available data for aspartate transport by Glt_{Ph}.

Results

To study the kinetic mechanism of Na^+-coupled aspartate transport by Glt_{Tk}, we used a classical enzymology method, in which we measured the initial uptake rates of radiolabelled L-aspartate into proteoliposomes reconstituted with purified Glt_{Tk}, as a function of the external concentrations of L-aspartate and Na^+. To ensure initial rate conditions, aspartate and Na^+ were absent from the lumen of the liposomes at the onset of the experiment, and the rate was determined from the linear part of the uptake experiment (Figure S1). In the first set of experiments, we measured the combined transport activity of proteins with right-side-out and inside-out membrane orientation in the liposomes, as we did not inactivate either of the two populations. These experiments can be compared with binding experiments performed in detergent-solution where the sidedness is absent. In follow-up experiments, we silenced one of the two populations which allows for comparison with experiments in which the transporters had been fixed in a single orientation by crosslinking [35,36].

We managed to determine accurate transport rates using external Na^+ concentrations in the range between 5 and 300 mM and of aspartate concentrations between 50 nM and 100 µM (Table 1). The upper and lower boundaries of the concentration ranges were set by practical considerations. Aspartate concentrations higher than 100 µM required large dilution of the radiolabelled amino acid with unlabelled aspartate, which caused poor signal-to-noise levels in the uptake experiments. Na^+ concentrations higher than 300 mM could not be used, because preparation of proteoliposomes in buffer containing high salt concentrations prevented formation of a firm pellet when centrifuged, therefore making impossible to reach the necessary protein concentration for the experiments. In the low concentration regime, conditions in which 1 mM Na^+ was used in combination with aspartate concentrations lower than 1 µM resulted in poor signal-to-noise ratios. Despite these limitations, the range of concentrations was sufficient to provide insight in the kinetic mechanism.

The results of the uptake experiments are summarized in Table 1, where each row contains the initial rates of transport (v_o) at a fixed sodium concentration, but with increasing aspartate concentrations. When analysing v0 as a function of the aspartate concentration row-by-row, we found that rectangular hyperbolic functions fitted the data well (Figure 1A), which allowed for determination of the apparent maximal rates of transport (v_{max}^{Asp} (app)) and apparent Michaelis

Menten constants (K_M^{Asp} (app)) (Table 2). The superscript "Asp" indicates that the aspartate was varied, while the sodium concentration was kept constant (hence "apparent").

Each column in Table 1 contains the measured initial rates of aspartate transport at increasing Na^+ concentrations, while maintaining a fixed aspartate concentration. Analysis of these rates as a function of the Na^+ concentration, revealed sigmoidal dependencies (Figure 1B). The Hill equation was used to fit the data, yielding values for v_{max}^{Na} (app) and K_MNa (app) and the apparent Hill coefficient nHill (app) (Table 3). In this case, the superscript "Na" indicates sodium-dependent measurements, and "apparent" indicates that the measurements were done at a fixed L-aspartate concentration.

For interpretation of the uptake data in the framework of a kinetic model of transport, the apparent affinities for L-aspartate (K_M^{Asp} (app)) and the apparent maximal rates (v_{max}^{Asp} (app) and v_{max}^{Na} (app)) are the most informative parameters. K_MNa (app) and nHill (app) are less informative, and were not used further [38,40].

K_M analysis reveals a complex mechanism

Information on the kinetic mechanism is contained both in the dependence of the apparent affinity for aspartate K_M^{Asp} (app) on the Na^+ concentration, and in potential differences between K_M^{Asp} (app) and the equilibrium constant for L-aspartate binding (K_d^{Asp} (app)). Table 2 shows that K_M^{Asp} (app) was strongly dependent on the Na^+ concentration at concentrations below 50 mM Na^+. At Na^+ concentrations above 100 mM, K_M^{Asp} (app) became independent of the Na^+ concentration and levelled off to 0.7 µM (Table 2), a value that is important for mechanistic interpretation (discussed in detail below).

Comparison of the K_M^{Asp} (app) values with the equilibrium constants for L-aspartate binding (K_d^{Asp} (app)), determined previously by isothermal titration calorimetry (ITC) in detergent solution [15], revealed almost identical values at a Na^+ concentration of 100 mM, but large differences at higher and lower concentrations of Na^+ (Figure 2). While K_M^{Asp} (app) was an order of magnitude higher than the equilibrium constant for binding at a sodium concentration of 300 mM (7.0×10^2 nM versus 75 nM), at concentrations below ~75 mM K_M^{Asp} (app) was up to an order of magnitude lower than the K_d^{Asp} (app). Such discrepancies are indicative of a complex kinetic mechanism that cannot be interpreted in the conceptual framework of the rapid equilibrium approximation, which is based

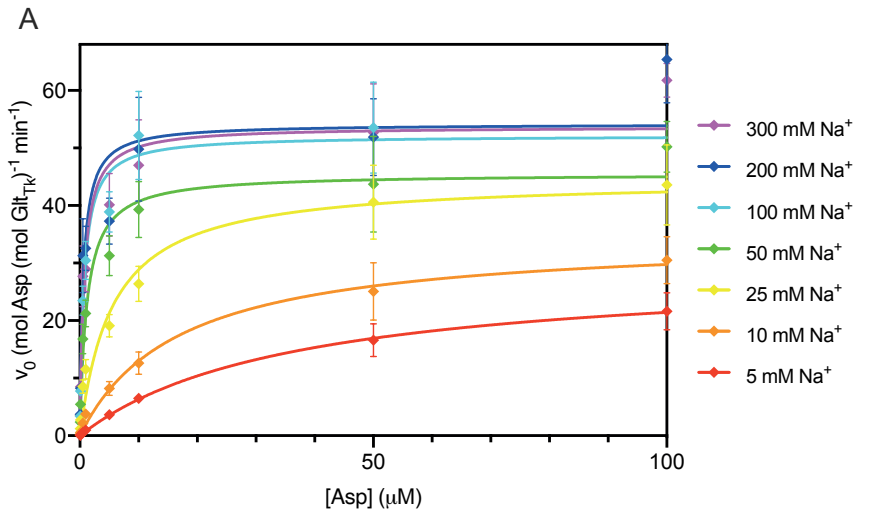

Figure 1: L-Asp transport rates catalysed by purified and reconstituted Glt_{Tk} as a function of the concentrations of Na^+ and L-aspartate. A. Aspartate-dependent measurements at different fixed Na^+ concentrations. The lines represent fits of the Michaelis Menten equation to the data for uptake at Na^+ concentrations of 5 mM (red), 10 mM (orange), 25 mM (yellow), 50 mM (green), 100 mM (cyan), 200 mM (blue), 300 mM (purple). B. Sodium-dependence of transport at fixed L-asp concentrations. The lines represent fits of the Hill equation to the data for uptake at 0.05 µM (red), 0.1 µM (orange), 0.5 µM (yellow), 1 µM (green), 5 µM (cyan), 10 µM (light blue), 50 µM (blue), 100 µM (purple). Each data point represents a triplicate measurement (n=3), and the standard error of the mean is shown.

on the assumption that the transport step (described by turnover number k_{cat}) is much slower than the establishment of the binding equilibrium of sodium ions and aspartate, described by the equilibrium constants K_d. The rapid equilibrium assumption was previously also dismissed for aspartate transport by Glt_{Ph}, based on more limited comparison of K_M and K_d [10], and on pre-equilibrium binding experiments in detergent solution [36], but the data presented here, based on the comparison of transport and binding experiments over a broad range of sodium concentrations, revealed a variable ratio between K_M^{Asp} (app) and K_d^{Asp} (app) depending on the Na^+ concentration, which is indicative of kinetic complexity.

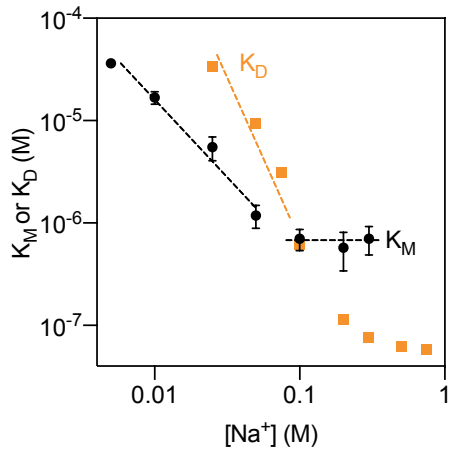

Figure 2: Dependence of the apparent affinities for L-Asp (K_M^{Asp} (app)) on the sodium ion concentration (black symbols). Dashed lines represent linear fits to datapoints in the low and high sodium ion concentration regimes. The standard error of the mean is shown (n=3). For comparison, the dissociation constants K_D^{Asp} (app) determined previously are also plotted (orange)[15].

Mechanistic interpretation of transport data using the Steady-state approximation

Because the rapid equilibrium approximation was found invalid, we turned to analysis based on the steady-state assumption. While the Michaelis-Menten or Hill equations can always describe the substrate dependencies of the uptake rates when the rapid equilibrium approximation is valid, it is possible to find more complex relations in the steady-state analysis, depending on the details of the kinetic mechanism [38]. For instance, for some kinetic mechanisms, v_{max} values may be (local) maxima, instead of being reached asymptotically, and K_M values may be undefined. Such complex relations often arise when steps occur

in the mechanism where two different substrates (corresponding to aspartate and Na^+ in the case of Glt_{Tk}) bind randomly [38]. In our data, the concentration dependences of the initial rates are described well by rectangular hyperbola and sigmoidal curves (Figure 1 and 2), suggesting that such random steps do not play a significant role, at least not in the concentration regime that we used. This notion is consistent with the kinetic binding model derived for detergent-solubilized Glt_{Ph}, where the binding of sodium ions and aspartate to Glt_{Ph} was found to be ordered in the concentration range between 5 and 300 mM Na^+, with two sodium ions binding before and one after aspartate [36]. This ordered binding mechanism is also consistent with a recent study that revealed a conformational selection step leading to binding of the first sodium ion [34]. Therefore, we chose to analyze the transport data presented here with the following kinetic model:

$$E \underset{k_{-1}}{\overset{k_1[Na^+]}{\rightleftarrows}} \{ENa\} \underset{k_{-2}}{\overset{k_2[Na^+]}{\rightleftarrows}} \{ENaNa\} \underset{k_{-3}}{\overset{k_3[Asp]}{\rightleftarrows}} \{ENaNaAsp\} \underset{k_{-4}}{\overset{k_4[Na^+]}{\rightleftarrows}} \{ENaNaAspNa\} \xrightarrow{k_{cat}} \quad (1)$$

in which E represents Glt_{Tk}.

While we base our further analysis on the mechanism shown in equation (1), we will show in the discussion section that the main conclusions hold for any mechanism in which at least one sodium ion binds after aspartate.

To derive a rate equation for this kinetic model of equation (1), we used the King Altman method [38,41]:

$$\frac{v_0}{v_{max}} = \frac{a_1[Na]^3[Asp]}{a_1[Na]^3[Asp] + a_2[Na]^2[Asp] + a_3[Na][Asp] + a_4[Na]^3 + a_5[Na]^2 + a_6[Na] + a_7} \quad (2)$$

in which v_{max} is the maximal attainable rate of transport at high Na^+ and L-aspartate concentrations, and a1- a7 are expressions of rate constants:

$$a_1 = k_1k_2k_3k_4 \quad (3)$$

$$a_2 = k_2k_3k_4k_{cat} + k_1k_3k_4k_{cat} + k_1k_2k_3k_{cat} + k_1k_2k_3k_{-4} \quad (4)$$

$$a_3 = k_{-1}k_3k_4k_{cat} \quad (5)$$

$$a_4 = k_1k_2k_4k_{cat} \quad (6)$$

$$a_5 = k_1 k_{-2} k_4 k_{cat} + k_1 k_2 k_{-3} k_{cat} + k_1 k_2 k_{-3} k_{-4} \quad (7)$$

$$a_6 = k_1 k_{-2} k_{-3} k_{cat} + k_{-1} k_{-2} k_4 k_{cat} + k_1 k_{-2} k_{-3} k_{-4} \quad (8)$$

$$a_7 = k_{-1} k_{-2} k_{-3} k_{cat} + k_{-1} k_{-2} k_{-3} k_{-4} \quad (9)$$

Equation (2) can be rearranged to derive expressions for v_{max}^{Na} (app) and v_{max}^{Asp} (app):

$$v_{max}^{Asp}(app) = v_{max} * \frac{a_1[Na]^2}{a_1[Na]^2 + a_2[Na] + a_3} \quad (10)$$

$$v_{max}^{Na}(app) = v_{max} * \frac{[Asp]}{\frac{a_4}{a_1} + [Asp]} = v_{max} * \frac{[Asp]}{\frac{k_{cat}}{k_3} + [Asp]} \quad (11)$$

Thus, the model predicts that both v_{max}^{Na} (app) and v_{max}^{Asp} (app) are dependent on the concentration of the other substrate, which is fully consistent with the data presented in Figure 3A and B. Moreover, equation (11) describes a rectangular hyperbolic relation between v_{max}^{Na} (app) and [Asp]. By fitting the Michaelis Menten equation to the data (Figure 3A), we found a value for k_{cat}/k_3 of 0.7 µM. Since the turnover number k_{cat} is known from the v_{max} data (~0.9s^{-1} (~54 min^{-1}), see Figure 3, Table 2), a value of ~1.3×10^6 $M^{-1}s^{-1}$ for k_3 is derived, remarkably similar to the value of 1.2×10^6 $M^{-1}s^{-1}$ that was found for Glt_{Ph}, obtained in pre-equilibrium binding experiments [36].

Equation (2) can also be rearranged to derive an expression for K_M^{Asp} (app):

$$K_M^{Asp}(app) = \frac{a_4[Na]^3 + a_5[Na]^2 + a_6[Na] + a_7}{a_1[Na]^3 + a_2[Na]^2 + a_3[Na]} \quad (12)$$

From equation (12) the values for K_M^{Asp} (app) that are reached in the low and high [Na^+] regimes can be found:

$$\lim_{[Na]\to\infty} K_M^{Asp}(app) = \frac{a_4}{a_1} = \frac{k_{cat}}{k_3} \quad (13)$$

$$\lim_{[Na]\to 0} K_M^{Asp}(app) = \frac{a_7}{a_3[Na]} \quad (14)$$

Equation (13) predicts that in the high concentration limit a constant value for K_M^{Asp} (app) is reached, which equals the ratio between two rate constants k_{cat}/k_3. The data presented in Figure 2 and Table 2 show that the value of K_M^{Asp} (app) levels off to ~0.7 µM at high Na^+ concentration. Since the turnover number k_{cat} is ~0.9s^{-1} (Figure 3, Table 2), a value of ~1.3×10^6 $M^{-1}s^{-1}$ for k_3 is found. Thus, two approaches (analysis of v_{max}^{Na} (app) and K_M^{Asp} (app)), reveal a value for k_3 that agrees well with the value of 1.2×10^6 $M^{-1}s^{-1}$ that was found for Glt_{Ph}.

When the apparent affinity constants are plotted in a double logarithmic plot against the concentration of Na^+, linear relations are approached in both the high and low Na^+ concentration extremes (Figure 2). The slope is zero at high Na^+ concentration (because K_M^{Asp} (app) levels off to k_{cat}/k_3), and a slope of -1.4 is found in the low Na^+ concentration regime, which deviates from the slope of -1 predicted by the model. This discrepancy may indicate that lower concentrations of sodium should have been used to meet the conditions for equation (14) to be valid, something which was impossible for technical reasons, as discussed above. Alternatively, the deviation might be caused by the experimental error inherent to the transport measurements at low Na^+ concentrations. The slope of the $logK_M$ plot in the low Na^+ concentration regime is ~ 2-fold shallower than that of the $logK_d$ plot, which is consistent with the binding model [36].

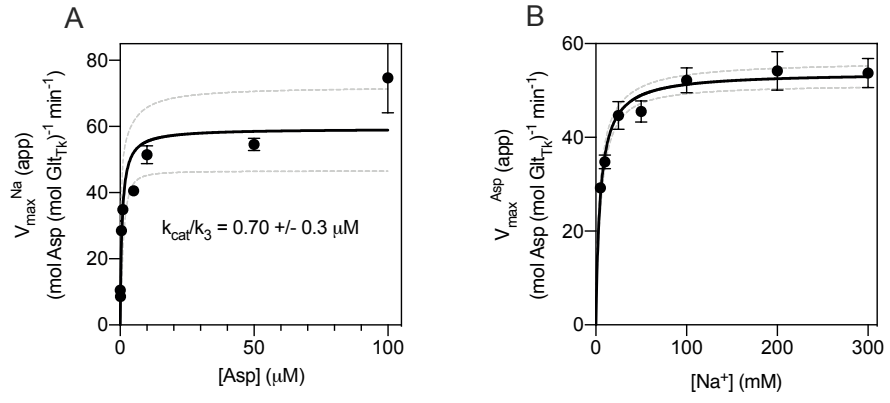

Figure 3: Dependence of the maximal rates L-Asp transport rate on the concentrations of Na^+ and L-aspartate. A. Dependence of the maximal rates of transport v_{max}^{Na} (app) from Figure 1A on the concentration of sodium ions. B. Dependence of the maximal rates of transport v_{max}^{Asp} (app) from Fig 1B on the concentration of L-Asp. Solid and dashed lines represent fits of rectangular hyperbolic functions to the data and the 95% confidence intervals, respectively. In panel A the fitted value of k_{cat}/k_3 (equation (13)) is indicated. The standard error of the mean is shown (n=3)

Side specific inhibition with Sybody

Although the analysis presented above is internally consistent, as well as consistent with existing kinetic data for binding on Glt_{Ph}, there is a potential complication caused by the proteoliposome system used, because the reconstitution procedure usually results in a mix of inside-out- and right-side-out-oriented proteins in the bilayer. For instance, it has been demonstrated that Glt_{Ph} reconstitutes in the two orientations with equal probability [10]. If the oppositely oriented proteins take up aspartate via different kinetic mechanisms (the equivalence of different mechanisms for forward and reverse transport in vivo), the results of the kinetic analysis could be convoluted and potentially lead to misinterpretation.

To determine to which extent the kinetic mechanism depends on the orientation of Glt_{Tk} in liposomes, we set out to inactivate either the right-side-out or the inside-out oriented transporters. Inhibition of the transporter from only one side of the membrane by modification of cysteine mutants did not work for Glt_{Tk}, possibly because of the one-gate nature of the elevator mechanism, in which identical binding site residues and gating elements are alternately exposed to either side of the membrane [13]. Therefore, we chose to explore an alternative method by using synthetic nanobodies (Sybodies) [39,42]. Since sybodies recognize water-exposed surface epitopes and are membrane impermeable, they are expected to be suitable for orientation-specific inhibition. We selected 42 unique sybodies against Glt_{Tk}, using an established platform, which included ribosome display, two rounds of phage display and ELISA [39].

One of these sybodies (Sybody 1) completely blocked aspartate transport by Glt_{Tk} when added from both sides of the membrane (in the lumen and in the external solution), but inhibited partially when added only on the outside of the proteoliposomes (Figure 4A). This sybody thus showed the characteristics of the sought-after sidedness of inhibition, and the result suggests that Glt_{Tk} was reconstituted in both orientations in the proteoliposomes, similar to what was shown for Glt_{Ph} before. To explain the inhibitory properties of Sybody 1, we solved a single particle cryo-EM structure of the sybody-Glt_{Tk} complex. The sybody binds on the extracellular surface of Glt_{Tk} at the interface between the transport and scaffold domain. The bound sybody thereby makes the elevator movement impossible, which prevents transport (Figure 4B). The sybody thus inactivates the Glt_{Tk} molecules with right-side-out orientation, and the residual uptake activity can be attributed to the inside-out oriented proteins.

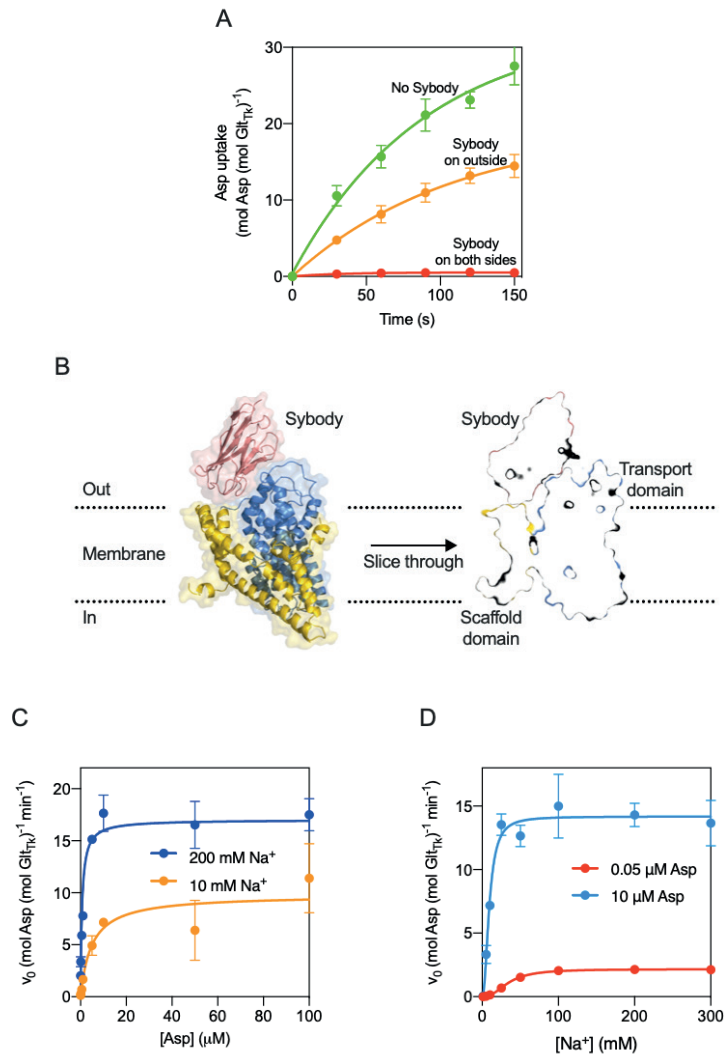

Figure 4: Inhibition of aspartate transport by the Sybody. A. Uptake of aspartate in liposomes reconstituted with Glt_{Tk} using aspartate and Na^+ concentrations of 1 μM and 300 mM respectively. Uptake traces in the absence of sybody (green), in the presence of 750 nM sybody on the outside (orange) or with sybody present on both sides of the membrane (red). Each data point represents a triplicate measurement (n=3), and the standard error of the mean is shown. B. Cryo-EM structure of the Glt_{Tk}-sybody complex. Left: cartoon representation of a Glt_{Tk} protomer (transport domain in blue and the scaffold in yellow) with sybody bound (red). The surface of the protein is shown in transparent representation, and the approximate location of the membrane boundaries are indicated with dashed lines. Right: Sliced-through representation highlighting that the sybody likely blocks movement of the transport domain along the scaffold domain. The transport domain is in the intermediate-outward state, as described in ref.[13] C and D. Same as in Figure 1A and 1B for a selection of conditions (using the same color coding), but now in the presence of 750 nM sybody on the outside of the liposomes.

We chose to use this sybody, added only on the outside of the proteoliposomes, to repeat a subset of the experiments described above. First, we tested whether v_{max}^{Na} (app) still depended on the aspartate concentration, and whether v_{max}^{Asp} (app) still depended on the Na^+ concentration when the right-side-out oriented molecules were inactivated by the sybody. Indeed, both v_{max} (app) values still varied with the concentrations of the co-substrate (Figure 4CD), consistent with the kinetic mechanism (equations (10) and (11)). Second, we determined whether a constant value for K_M^{Asp} (app) was still reached in the high Na^+ concentration limit, as predicted by Equation (13). Indeed, a constant value of ~0.6 µM found was found above 100 mM Na^+, which intriguingly did not deviate significantly from the value in the dual-population proteoliposomes (Table 5). Assuming that the k_{cat} value of the active population of inside-out oriented proteins was still ~0.9s^{-1}, the value of k_3 remained unaltered. In other words, the measurable parameters of the kinetic mechanism of the right-side-out and inside-out oriented proteins were very similar.

Discussion

Reconstitution of purified membrane proteins in liposomes often leads to mixed orientation in lipid bilayers. For secondary active transporters, which can readily operate in both directions, the co-existence of right-side out and inside out oriented proteins is problematic for kinetic analysis. The work presented here shows that inactivation of a transporter from one side of the membrane using a synthetic nanobody (Sybody) is an effective way to deal with mixed orientation upon reconstitution in liposomes [39,42]. Synthetic nanobodies are membrane impermeable, and highly specific for the binding epitope. While also natural nanobodies could be used for this purpose, sybodies offer a major advantage, because the selection can be carried out under defined buffer conditions, which may be used to steer the selection towards binders of a specific state. Also, the method of immobilization used in the ribosome and phage display steps can be used to create bias for binders to the external or internal surface of the transporters. Finally, the generation of sybodies is quicker compared to nanobody generation, requires less protein, and does not require animal handling.

Here, the inactivation of the population of right-side out oriented Glt_{Tk} by sybody binding made it possible to analyze uptake catalyzed by inside-out oriented proteins. The aspartate transport rates obtained in the presence of the sybody can be compared directly with a previous pre-equilibrium binding study on detergent-solubilized Glt_{Ph}. In the latter study, the transporter was fixed in the inward-oriented state by Hg2+-crosslinking of a double cysteine mutant, which allowed for determination of the kinetic mechanism of binding of sodium ions and aspartate, and estimation of rate constants for association and dissociation [36]. In our study, where we used a sybody to inactivate the population of right-side-out oriented Glt_{Tk} transporters in proteoliposomes, we measured the kinetics of the reversed transport step, which includes binding of Na^+ and aspartate to the inward-oriented state similar to the pre-equilibrium binding study. In the Na^+ concentration range between 5 and 300 mM, the two studies are fully congruent, and consistent with a mechanism in which two sodium ions bind first, followed by aspartate and finally the last sodium ion. The kinetic analysis presented here shows that the rate constant for association of aspartate (k_3 in equation (1)), can be obtained using equation (13), when K_M^{Asp} (App) is determined in the limit of high Na^+ concentrations (as shown in Figure 2) and the turnover number k_{cat} is taken directly from the maximally attainable rate at high Na^+ and aspartate concentrations (v_{max}). The value for k_3 derived in this way was $1.3\times10^6 M^{-1}s^{-1}$, which closely matches the value of $1.2\times10^6 M^{-1}s^{-1}$ for Glt_{Ph} derived from pre-equilibrium binding experiments [36].

More importantly, it is also possible to determine the turnover number k_{cat} using the same analysis, if k_3 is known from binding experiments (which is the case for Glt_{Ph}). This notion is relevant, because quantification of the amount of transport protein present in membranes is often difficult, making direct determination of k_{cat} from v_{max} values notoriously error-prone, which can be easily illustrated by the available data on Glt_{Ph}: For aspartate transport by Glt_{Ph}, the value for K_M^{Asp}(app) at 100 mM Na^+ has been determined accurately (120 nM) [43]. Assuming that this Na^+ concentration is sufficiently high to represent the limit where K_M^{Asp}(app) has become constant, and using the k_3 value of $1.2\times10^6 M^{-1}s^{-1}$ determined by pre-equilibrium binding, from equation (13) a k_{cat} value of 0.14s^{-1} is calculated. It is important to emphasize that this value has been derived without using error-prone determination of the protein concentration in the transport assay. For comparison, if k_{cat} is derived directly from the v_{max} value of 3.4 nmol×mg^{-1}×min^{-1}, a value of $2.6\times10^{-3}s^{-1}$ is found [43]. The huge discrepancy between the two values is probably caused by inaccurate protein concentration determination in the proteoliposomes, or loss of activity during the reconstitution process.

It is noteworthy that in the experiments on Glt_{Tk} presented here, the k_3 value of $1.3\times10^6 M^{-1}s^{-1}$ that we determined from the measurement of K_M^{Asp} (app) and k_{cat}, was remarkably similar to the experimentally determined value of k_3 for Glt_{Ph} of $1.2\times10^6 M^{-1}s^{-1}$ [36]. The virtually identical rates of aspartate association step in Glt_{Ph} and Glt_{Tk} are consistent with the structures of the binding sites in the two proteins, which are essentially the same [7–9,13,15,16,20,44]. Therefore, we believe that the Glt_{Tk} protein concentration, used to derive k_{cat}, was reasonably accurate in this case.

The 6-fold difference in turnover number k_{cat} between Glt_{Ph} and Glt_{Tk} ($0.14s^{-1}$ and $0.9s^{-1}$ respectively) could be caused by (small) structural differences away from the binding site. k_{cat} is not a single rate constant, but is composed of contributions from all steps that take place after binding of the last sodium ion in the catalytic cycle, until the binding of the first sodium ion in the next round of catalysis. These steps include movement of the fully loaded transport domain between outward- and inward-oriented states, opening of the binding site towards the lumen of the liposomes, release of the sodium ions and aspartate, occlusion of the empty binding site in the apo state, movement of the transport domain in the occluded apo state, opening of the binding site externally. The latter step also includes the rate constant for reshaping the binding sites for the first two sodium ions, leading to conformational selection that was shown to occur in Glt_{Ph} [34]. Therefore, differences between Glt_{Ph} and Glt_{Tk} that affect any of these steps may affect k_{cat}, which is observable in the value for K_M^{Asp} (app) at high sodium concentrations.

The origin of the differences between Glt_{Ph} and Glt_{Tk} may be similar to that of differences between wild-type Glt_{Ph} and a faster "unlocked" mutant [18,43]. This mutant has the same value for k_3 as the wild-type[36], consistent with the observation that the structure of the binding site is identical to the wild-type. Therefore, determination of K_M^{Asp} (app) in the limit of high sodium ion concentration allows for derivation of accurate values for k_{cat}. The values for K_M^{Asp} (app) have been determined at 100 mM Na^+ for both wild-type Glt_{Ph} and the fast mutant (120 nM and 406 nM respectively)[43]. If we again assume that this Na^+ concentration is high enough to represent the limit where K_M^{Asp} (app) becomes constant for both proteins, then k_{cat} is predicted to be ~3.5 times higher in the fast mutant, which is in a good agreement with bulk transport data that showed ~4.5 fold difference in v_{max} values (although the absolute numbers are both far off for the reasons discussed above)[43].

While it is also possible to determine turnover numbers using a recently established transport assay at the single molecule level [45], derivation of a full kinetic mechanism by combining turnover numbers from single molecule transport measurements with rate constants determined in pre-equilibrium binding experiments, is not straightforward, because the latter are ensemble measurements. In pre-equilibrium binding experiments [33,34,36,37] and bulk transport experiments (presented here), the entire ensemble contributes to the measured rate constants, but in single molecule transport experiments, the k_{cat} is determined for only a fraction of the ensemble. It is difficult to account for the contribution of the all populations of (slightly) differently behaving individual proteins that together make up the ensemble. This is especially problematic for Glt_{Ph}, because this protein switches between active and quiescent modes, and may get stuck in kinetically distinct conformation by static disorder, all of which last for extended periods of time [45]. This may explain why the turnover numbers determined by single molecule transport experiments deviate from those determined by bulk experiment.

While the kinetic mechanism presented here is valid only for the reverse transport reaction (because we inactivated the forward-operating transporters by the sybody), it is well possible that the same mechanism is also used for the forward transport reaction. Similarity of the forward and reverse kinetic mechanisms is indeed supported by the essentially identical kinetic parameters in the presence and absence of the sybody. From a structural point of view this similarity can be explained because the transporter uses the same gating element on both sides of the membrane ("one-gate elevator"), and the binding site geometry and access path in the inward- and outward-oriented states are essentially the same [13,20,46,47]. In future experiments the kinetic mechanism for forward transport by Glt_{Tk} may be tested if we manage to inactivate the inside-out oriented population of Glt_{Tk} molecules by a suitable sybody.

In contrast to what we found for Glt_{Tk}, differences in the kinetic mechanisms of the forward and reverse reactions have been proposed for the mammalian glutamate transporter EAAC1 [48]. Although it is possible that the differences in kinetic mechanism between Glt_{Tk} and EAAC1 are real, it also possible that they are caused by differences in the readout of transport. While for Glt_{Tk} transport was measured directly (using radioactivity), for EAAC1 the substrate-induced chloride conductance was used as a readout. In addition, the analysis of the data for EAAC1 was based on the rapid-equilibrium assumption, which may

not be valid. Finally, the more limited range of co-ion concentrations tested for EAAC1 may have obscured mechanistic details.

In conclusion, analysis of the kinetic mechanism of sodium-coupled aspartate transport by Glt_{Tk} and Glt_{Ph} provides a way to determine accurate turnover numbers from K_M^{Asp} (app) values, without the need to use error-prone protein quantification. This is of great use for instance when analyzing the effects of mutations. Depending on the details of the kinetic mechanism, it may also be possible to determine turnover numbers in a similar way for other transport proteins. To test whether kinetic mechanisms different from the one analyzed here (equation (1)) would also allow for similar determination of the turnover number, we used the King-Altman method [38,41] to derive rate equations for all possible kinetic mechanisms leading to the coupled transport of three sodium ions and aspartate [40]. It turns out that if at least one sodium ion binds after aspartate, K_M^{Asp} (app) values in limit of high sodium concentration equal the ratio between k_{cat} and the on-rate for aspartate binding (as in equation (13)). It is also noteworthy that this even holds if multiple sodium ions bind randomly (for instance if steps 1 and 2 in equations (1) would be random). Therefore, it is likely that more transporters can be analyzed in the same way as presented here, and we conclude that systematic analysis of transport rates, and derivation of the rate equation, are essential steps in the elucidation of transport mechanisms.

Methods

Glt_{Tk} purification and reconstitution in proteoliposomes

Glt_{Tk} was produced in *E.coli* strain MC1061 with the L-arabinose inducible vector pBad24 as described in Arkhipova et al. (2019) [14]. The cells were grown in LB media supplemented with 100mg/L ampicillin. The expression was induced by addition of 0.05% L-arabinose when the culture reached 0.8 OD600. Three hours after induction the cells were harvested by centrifugation (7000 rpm, 15', 4°C Beckman JLA 9.1000) and resuspended in ice cold 20 mM Tris-HCl. The cells were lysed by means of a cell disruptor cooled to 4°C and operated at 25 PSI. The lysate went through an intermediate centrifugation (7500 RPM, 20', 4°C, Beckman JA25.50) step to remove cell debris, the supernatant was finally ultracentrifuged (40000 RPM 150', 4°C, Beckman 50.1 Ti) and the pellet was resuspended in 20 mM Tris-HCl pH 8 before storing the membrane vesicles at -80 °C.

The membrane vesicles were then added to solubilisation buffer (50 mM Tris-HCl pH8, 300 mM KCl, 1% DDM), incubated for 45' on a rocking platform at 4°C and finally centrifuged (55000 RPM, 30', 4°C, Beckman MLA 55) to separate the membranes from the solubilized protein. The supernatant was supplemented with 15 mM imidazole pH 8 and with 0.5 mL of Ni-Sepharose slurry pre-equilibrated with 50 mM Tris-HCl, 300 mM KCl. After 1h of incubation the mixture was loaded onto a Poly-Prep column and unbound protein was allowed to flow through. The column was washed with 20 column volumes of washing buffer (50 mM Tris-HCl, 300 mM KCl, 60mM imidazole, 0.15% DM) and finally eluted in three fractions of 300, 800 and 400 µL respectively using elution buffer (50 mM Tris-HCl, 300 mM KCl, 500mM imidazole, 0.15% DM). The second fraction was loaded onto a Superdex-200I gel filtration column equilibrated with 10mM HEPES pH 8, 100 mM KCl and 0.15%DM. The final concentration of the purified protein was determined by measuring the absorbance at 280nm (Glt_{Tk} ε=37360).

The lipids used to reconstitute Glt_{Tk} contained a 3:1 mixture of *E.coli* lipid polar extract and egg phosphatidylcholine (PC) (Avanti). Liposomes were homogenized by extruding 11 times through a 400 nm pore size polycarbonate filter and subsequently diluted to 5 mg/mL in 50 mM potassium phosphate buffer (pH 7.0). To allow the insertion of the protein into the bilayer, the lipids were destabilized by step-wise addition of 10% Triton X-100 while scattering was followed at a wavelength of 540 nm. The titration was stopped once the absorption signal decreased to about 60% the maximum value reached. Purified protein was added at a protein:lipid ratio (w/w) of 1:1600. The protein lipid mixture was incubated for 30' at RT, and then the detergent was removed by addition of BioBeads in three steps: First 15 mg/mL BioBeads were added followed by incubation for 60' at 4°C, then 19 mg/mL BioBeads were added followed by overnight incubation at 4°C. Finally, 29 mg/mL BioBeads were added followed by 120'incubation at 4°C. BioBeads were then removed and the proteoliposomes were pelleted (80,000 RPM, 25', 4°C, Beckman MLA80) and resuspended in 50 mM potassium phosphate buffer (pH 7) to a final lipid concentration of 20 mg/ml. The proteoliposomes were subjected to three cycles of freeze-thawing using liquid nitrogen and stored until use.

Sybody selection

Sybodies were selected against two Glt_{Tk} cysteine mutants (298C and 367C), which while biotinylated and immobilized during the selection procedures would make both extracellular and intracellular epitopes accessible for binding.

Selection was done in the presence of 50 µM L-aspartate, 150 mM NaCl and 0.15% DM according to an established in vitro selection platform that included ribosome display, two rounds of phage display and ELISA (Zimmermann et al., 2018, 2020). During ELISA, every single clone was analyzed for binding against Glt_{Tk} in the presence and absence of L-aspartate. Sequencing of 48 ELISA positive hits resulted in 42 unique sybody sequences (20 for the 298C mutant and 22 for the C367 mutant).

Sybody expression and purification

Each of 42 sybodies was expressed in *E.coli*, purified from the periplasm using Ni^{2+}-affinity chromatography and analyzed by size exclusion chromatography (SEC). Based on the quality of the SEC profiles (absence of aggregates, no interactions with column material, high yield) we selected 33 purified sybodies (14 for the 298C mutant and 19 for the 367 C mutant), which were tested for their ability to inhibit Glt_{Tk} transport of aspartate in uptake assays. For large scale purification of inhibitory Sybody 1, a preculture of *E.coli* MC1061 transformed with pSB_initSB1 was used to inoculate 50 mL of TB medium supplemented with 25 ug/ml chloramphenicol. The culture was grown for 2h at 37°C while shaking at 200 rpm, the temperature was then lowered to 22°C and let grow until OD ~0.8. The expression was induced by adding L-arabinose to a final concentration of 0.02% and let express overnight at 22°C while shaking. Cells were pelleted and resuspended in 5 mL periplasmic extraction buffer (20% sucrose (w/v) 50 mM Tris-HCl (pH 8.0), 0.5 mM EDTA and 0.5 ug/ml Lysozyme) and incubated on ice for 30 minutes, after incubation 20 mL of TBS (20mM Tris-HCl (pH 7.4) 150 mM NaCl) supplemented with 1 mM MgCl2 were added. The lysate was centrifuged at 4,000g for 20 minutes and the supernatant was transferred in a tube containing 500 µL of Ni-sepharose pre-equilibrated in TBS and supplemented with imidazole to a final concentration of 15 mM. After 1h incubation on a shaking platform, the solution containing the SyBody was applied to a polyprep gravity column and the unbound fraction was let flow through. The resin was then washed with 10 CV of TBS supplemented with 30 mM imidazole and eluted in 500 ul of TBS supplemented with 300 mM imidazole. The Sybody solution was then passed through a NAP-10 column equilibrated with the internal uptake buffer (10 mM potassium phosphate buffer (pH 7), 300 mM KCl) and stored at -80°C. Sybody 1 was selected from the library created by the mutant 298C.

Transport assay

The lumenal buffer in each proteoliposome preparation was changed to 10 mM potassium phosphate buffer (pH 7) and 300mM KCl. For this, the proteoliposomes were first pelleted (80,000 RPM, 25', 4°C, Beckman MLA80) and then resuspended in the lumenal buffer. After three freeze-thaw cycles the suspension was extruded 11 times through a polycarbonate filter with 400-nm pore size in order to obtain homogeneously sized unilamellar vesicles which were pelleted (80000 RPM, 25', 4°C, Beckman TLA100.3) and resuspended to a final lipid concentration of 100 mg/mL.

To completely inhibit aspartate transport of Glt_{Tk} by Sybody 1 (on both sides of the membrane) the lumenal solution was supplemented with 150 µM of Sybody 1. After performing 6 freeze-thaw cycles, and extrusion (11 times) through a polycarbonate filter with 400-nm pore size, the homogeneous solution was pelleted (80000 RPM, 20', 4°C, Beckman TLA100.1) and resuspended to a final lipid concentration of 100 mg/mL in a solution containing 75 µM of Sybody 1, 10 mM potassium phosphate buffer (pH 7) and 300 mM KCl.

To inhibit only the right side-out fraction of Glt_{Tk} a homogeneous solution of proteoliposomes was prepared as described above (with luminal buffer devoid of Sybody) and after pelleting by ultracentrifugation it was resuspended to a final lipid concentration of 100 mg/mL with a solution containing 75 µM of Sybody 1, 10 mM potassium phosphate buffer (pH 7) and 300 mM KCl.

To start the transport the proteoliposome suspension was diluted 100 fold into external buffer while stirring. The external buffer contained 10 mM potassium phosphate buffer (pH 7), 3 µM valinomycin, 1 – 300 mM NaCl, 0.05 – 100 µM L-aspartate; to balance the osmotic strength with that of the luminal solution, choline chloride was added (Table 1). In case the Sybody was present, the 100-fold dilution resulted in a final external concentration of Sybody of 750 nM.

After the indicated incubation period (20s for the data in Figure 1 and 4CD), 2 mL of ice-cold quenching buffer (10 mM potassium phosphate (pH 7), 300 mM KCl) was added. The content of the tube was then poured onto a BA 45 nitrocellulose filter which was then washed with 2 mL of quenching buffer. The filters finally dissolved in scintillation cocktail Ultima Gold (Perkin Elmer) and the β-decay from the radiolabeled substrate was counted. The time-point zero measurement for each condition was measured by pipetting the liposome suspension on the side of a test tube containing 200 µL of reaction buffer

and subsequently flushing them in the reaction buffer with 2 mL of ice-cold quenching buffer (10 mM potassium phosphate (pH 7), 300 mM KCl).

The value for each uptake rate represents the average and standard error of three independent biological replicates, each constituted by two or three technical replicates. The substrate-dependent uptake rates obtained at fixed concentration of Na^+ were plotted as a function of L-aspartate and fitted to the Michaelis-Menten equation to obtain apparent K_M (K_M^{Asp} (app)) and v_{max} (v_{max}^{Asp} (app)) values for different [Na^+]. The co-ion dependent uptake rates obtained at a fixed concentration of L-aspartate were plotted as a function of Na^+ and fitted to the Hill equation of obtain K_M (K_MNa (app)), v_{max} (v_{max}^{Na} (app)) and nHill values for different [L-Asp]. The statistical analysis of the data was executed in GraphPad Prism 9.

Single particle Cryo-EM

The structure of Glt_{Tk} in complex with Sybody 1 (molar ratio 3:1) was determined using essentially the same protocol as described in Arkhipova et al 2020[13], in the presence of 300 mM Na^+ and 50µM L-Asp. The purified complex at the concentration of 0.5-1 mg/ml was applied onto freshly glow-discharged Quantifoil grids (Au R1.2/1.3, 300 mesh) at 22°C and 100% humidity and plunged-frozen in liquid ethane. The Cryo-EM data were collected using 200-keV Talos Arctica microscope (Thermo Fisher). Cryo-EM image processing was performed using cryoSPARC software [49].

In brief, 824 micrographs were selected for the processing after motion correction and CTF estimation. The template for particle picking was generated from 100 manually picked particles. Template-based picking identified 109217 particles. Subsequent 2D classification reduced the number of particles to 67498 and subsequently 53983 particles were left in the selected ab initio class. Final non-uniform 3D refinement resulted in a 3.5 Å map (with C1 symmetry applied), which was sharpened using Autosharpen Map procedure in Phenix [50] and used for model building using Coot [51]. The refinement of the coordinates was performed in realspace refine module of Phenix [52]. The data collection and refinement statistics are shown in Table 5. Visualization and structure interpretation were carried out in UCSF Chimera [53] and PyMol (Schrödinger, LLC).

Supplementary data & Tables

Table 1: Initial rates of L-Aspartate uptake by Glt_{Tk} reconstituted in proteoliposomes. In the first column, the concentrations in parentheses indicate the amount of choline chloride used in the external reaction buffer to balance the osmotic and ionic strength. The standard error of the mean is indicated (n=3)

[L-Asp]→ [Na^+↓]	**0.05 µM**	**0.1 µM**	**0.5 µM**	**1 µM**	**5 µM**	**10 µM**	**50 µM**	**100 µM**
1 mM (299 mM)	not determined	not determined	not determined	0.03 ±2.6 10^{-2} min^{-1}	0.51 ±0.3 min^{-1}	0.25 ±0.3 min^{-1}	2.85 ±1.2 min^{-1}	10.93 ±4.4 min^{-1}
5 mM (295 mM)	0.05 ±1.6 10^{-2} min^{-1}	0.06 ±2.1 10^{-2} min^{-1}	0.59 ±0.1 min^{-1}	0.96 ±0.2 min^{-1}	3.62 ±0.7 min^{-1}	6.48 ±0.9 min^{-1}	16.59 ±2.8 min^{-1}	21.62 ±3.2 min^{-1}
10 mM (290 mM)	0.21 ±5.5 10^{-2} min^{-1}	0.28 ±0.1 min^{-1}	2.16 ±0.4 min^{-1}	3.75 ±0.6 min^{-1}	8.19 ±1.2 min^{-1}	12.60 ±1.9 min^{-1}	25.08 ±5.0 min^{-1}	30.51 ±4.1 min^{-1}
25 mM (275 mM)	0.95 ±0.2 min^{-1}	1.46 ±0.5 min^{-1}	8.53 ±1.2 min^{-1}	11.56 ±1.7 min^{-1}	19.09 ±2.0 min^{-1}	26.39 ±3.0 min^{-1}	40.58 ±6.4 min^{-1}	43.59 ±6.9 min^{-1}
50 mM (250 mM)	1.88 ±0.4 min^{-1}	3.34 ±1.0 min^{-1}	16.79 ±2.6 min^{-1}	21.26 ±2.3 min^{-1}	31.28 ±3.5 min^{-1}	39.30 ±4.9 min^{-1}	43.69 ±8.3 min^{-1}	50.21 ±4.4 min^{-1}
100 mM (200 mM)	2.75 ±0.5 min^{-1}	4.79 ±1.5min^{-1}	23.46 ±2.5 min^{-1}	30.47 ±3.3 min^{-1}	38.90 ±3.5 min^{-1}	52.16 ±7.7 min^{-1}	53.52 ±7.9 min^{-1}	68.13 ±3.5 min^{-1}
200 mM (100 mM)	3.06 ±0.6 min^{-1}	4.83 ±1.5 min^{-1}	31.27 ±6.4 min^{-1}	32.55 ±3.8 min^{-1}	37.29 ±4.0 min^{-1}	49.80 ±9.0 min^{-1}	51.90 ±6.7 min^{-1}	65.40 ±7.5 min^{-1}
300 mM (0 mM)	2.93 ±0.7 min^{-1}	4.96 ±1.6 min^{-1}	27.72 ±5.3 min^{-1}	28.95 ±4.0 min^{-1}	40.12 ±5.4 min^{-1}	46.98 ±7.9 min^{-1}	52.69 ±8.5 min^{-1}	61.77 ±2.9 min^{-1}

Table 2: v_{max}^{Asp} (app) and K_M^{Asp} (app) values for aspartate dependent uptakes obtained at constant [Na^+] (From Figure 1A). The standard error of the mean is indicated (n=3)

[Na^+]	v_{max}^{Asp} (app) (min^{-1})	K_M^{Asp} (app) (μM)
5 mM	29.2 ± 0.58	36 ± 1.9
10 mM	34.8 ± 1.5	16.8 ± 2.4
25 mM	44.7 ± 2.9	5.5 ± 1.5
50 mM	45.5 ± 2.3	1.2 ± 0.3
100 mM	52.1 ± 2.6	0.70 ± 0.16
200 mM	54.2 ± 4.1	0.58 ± 0.23
300 mM	53.7 ± 3.1	0.70 ± 0.22

Table 3: v_{max}^{Na} (app), K_M^{Na} (app) and n_{Hill} (app) values for Na^+ dependent uptakes obtained at constant [Asp] (from Figure 1B). The standard error of the mean is indicated (n=3)

[L-Asp]	v_{max}^{Na} (app) (min^{-1})	K_M^{Na} (app) (mM)	n_{Hill} (app)
0.05 μM	3.7 ± 0.1	36.7 ± 1.8	2.1 0.19
0.1 μM	8.6 ± 0.1	37.0 ± 0.81	2.0 ± 0.08
0.5 μM	28.5 ± 0.15	40.9 ± 0.42	1.70 ± 0.025
1 μM	34.9 ± 1.0	37.3 ± 2.0	1.7 ± 0.13
5 μM	40.6 ± 1.3	24.7 ± 2.1	1.6 ± 0.19
10 μM	51.4 ± 2.7	21.8 ± 3.2	1.5 ± 0.29
50 μM	54.6 ± 1.9	10.9 ± 1.2	1.1 ± 0.14
100 μM	72.34 ± 10.5	14.8 ± 7.9	0.72 ± 0.21

Table 4: v_{max}^{Asp} (app) and K_M^{Asp} (app) values for aspartate dependent uptakes obtained at constant [Na^+] in the presence of 750 nM sybody on the outside of the liposomes. The standard error of the mean is indicated (n=3)

[Na^+]	v_{max}^{Asp} (app) (min^{-1})	K_M^{Asp} (app) (μM)
10 mM	9.8 ± 1.0	4.9 ± 1.4
100 mM	18.3 ± 2.0	0.97 ± 0.36
200 mM	17.0 ± 1.0	0.65 ± 0.13
300 mM	17.2 ± 1.5	0.63 ± 0.17

Table 5: Cryo-EM data collection, refinement and validation

Data collection and processing	
Voltage (kV)	200
Electron exposure ($e^-/Å^2$)	53.3
Defocus range (μm)	-0.5 to -2.0
Pixel size (Å)	1.012
Symmetry imposed	C1
Initial dataset (# of particles)	109217
Final dataset (# of particles)	53983
Map resolution (Å) $FSC_{0.143}$	3.5
Refinement	
Initial model used	PDB 6XWQ
Model composition	
Nonhydrogen atoms	10357
Protein residues	1378
Ligands	3
Mean B factors ($Å^2$)	
Protein	160.2
Ligand	165.8
R.m.s. deviations	
Bond lengths (Å)	0.005
Bond angles (°)	0.635
Validation	
MolProbity score	2.09
Clash score	17.7
Poor rotamers (%)	0.00
Ramachandran plot (%)	
Favoured	95.07
Allowed	4.93
Outliers	0.00
Model to map fit CC	0.86

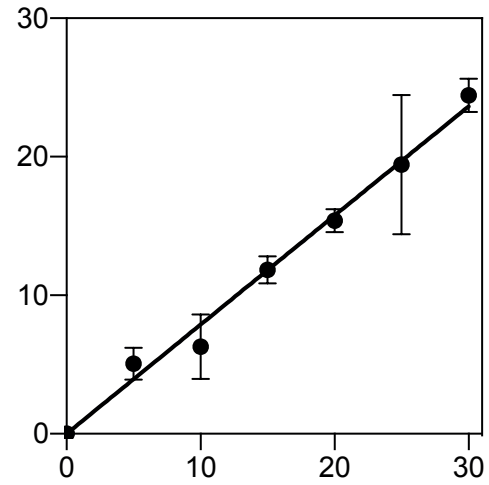

Figure S1: Time course of aspartate uptake in proteoliposomes with reconstituted Glt_{Tk}. v_{max} conditions were used (300 mM Na^+ and 100 μM L-Aspartate). The experiment was done in triplicate with the error representing the standard deviation. From this result we concluded that the transport rate is constant over the first 30 seconds of the experiment.

References

1. Danbolt NC: **Glutamate uptake**. *Prog Neurobiol* 2001, **65**:1–105.
2. Kanner BI, Sharon I: **Active Transport of L-Glutamate by Membrane Vesicles Isolated from Rat Brain**. *Biochemistry* 1978, doi:10.1021/bi00612a011.
3. Freidman N, Chen I, Wu Q, Briot C, Holst J, Font J, Vandenberg R, Ryan R: **Amino Acid Transporters and Exchangers from the SLC1A Family: Structure, Mechanism and Roles in Physiology and Cancer**. *Neurochem Res* 2020, doi:10.1007/s11064-019-02934-x.
4. Jensen AA, Fahlke C, Bjørn-Yoshimoto WE, Bunch L: **Excitatory amino acid transporters: Recent insights into molecular mechanisms, novel modes of modulation and new therapeutic possibilities**. *Curr Opin Pharmacol* 2015, **20**:116–123.
5. Zerangue N, Kavanaugh MP: **Flux coupling in a neuronal glutamate transporter**. *Nature* 1996, **383**:634–637.
6. Owe SG, Marcaggi P, Attwell D: **The ionic stoichiometry of the GLAST glutamate transporter in salamander retinal glia**. *J Physiol* 2006, **577**:591–599.
7. Yernool D, Boudker O, Jin Y, Gouaux E: **Structure of a glutamate transporter homologue from Pyrococcus horikoshii**. *Nature* 2004, **431**:811–818.
8. Jensen S, Guskov A, Rempel S, Hänelt I, Slotboom DJ: **Crystal structure of a substrate-free aspartate transporter**. *Nat Struct Mol Biol* 2013, **20**:1224–1227.
9. Boudker O, Ryan RM, Yernool D, Shimamoto K, Gouaux E: **Coupling substrate and ion binding to extracellular gate of a sodium-dependent aspartate transporter**. *Nature* 2007, **445**:387–393.
10. Ryan RM, Compton ELR, Mindell JA: **Functional characterization of a Na^+-dependent aspartate transporter from Pyrococcus horikoshii**. *J Biol Chem* 2009, **284**:17540–17548.
11. Kortzak D, Alleva C, Weyand I, Ewers D, Zimmermann MI, Franzen A, Machtens J, Fahlke C: **Allosteric gate modulation confers K + coupling in glutamate transporters** . *EMBO J* 2019, **38**:e101468.
12. Arkhipova V, Fu H, Hoorens MWH, Trinco G, Lameijer LN, Marin E, Feringa BL, Poelarends GJ, Szymanski W, Slotboom DJ, et al.: **Structural Aspects of Photopharmacology: Insight into the Binding of Photoswitchable and Photocaged Inhibitors to the Glutamate Transporter Homologue**. *J Am Chem Soc* 2021, doi:10.1021/jacs.0c11336.
13. Arkhipova V, Guskov A, Slotboom DJ: **Structural ensemble of a glutamate transporter homologue in lipid nanodisc environment**. *Nat Commun* 2020, **11**:998.
14. Arkhipova V, Trinco G, Ettema TW, Jensen S, Slotboom DJ, Guskov A: **Binding and transport of D-aspartate by the glutamate transporter homolog Glt_{Tk}**. *Elife* 2019, **8**:1–12.
15. Guskov A, Jensen S, Faustino I, Marrink SJ, Slotboom DJ: **Coupled binding mechanism of three sodium ions and aspartate in the glutamate transporter homologue Glt Tk**. *Nat Commun* 2016, **7**:1–6.
16. Reyes N, Ginter C, Boudker O: **Transport mechanism of a bacterial homologue of glutamate transporters**. *Nature* 2009, **462**:880–885.
17. Georgieva ER, Borbat PP, Ginter C, Freed JH, Boudker O: **Conformational ensemble of the sodium-coupled aspartate transporter**. *Nat Struct Mol Biol* 2013, doi:10.1038/nsmb.2494.
18. Akyuz N, Georgieva ER, Zhou Z, Stolzenberg S, Cuendet MA, Khelashvili G, Altman RB, Terry DS, Freed JH, Weinstein H, et al.: **Transport domain unlocking sets the uptake rate of an aspartate transporter**. *Nature* 2015, doi:10.1038/nature14158.
19. Ruan Y, Miyagi A, Wang X, Chami M, Boudker O, Scheuring S: **Direct visualization of glutamate transporter elevator mechanism by high-speed AFM**. *Proc Natl Acad Sci U S A* 2017, **114**:1584–1588.
20. Wang X, Boudker O: **Large domain movements through the lipid bilayer mediate substrate release and inhibition of glutamate transporters**. *Elife* 2020, doi:10.7554/eLife.58417.
21. Erkens GB, Hänelt I, Goudsmits JMHH, Slotboom DJ, Van Oijen AM: **Unsynchronised subunit motion in single trimeric sodium-coupled aspartate transporters**. *Nature* 2013, **502**:119–123.
22. Hänelt I, Wunnicke D, Bordignon E, Steinhoff HJ, Slotboom DJ: **Conformational heterogeneity of the aspartate transporter Glt Ph**. *Nat Struct Mol Biol* 2013, **20**:210–214.
23. Tanui R, Tao Z, Silverstein N, Kanner B, Grewer C: **Electrogenic steps associated with substrate binding to the neuronal glutamate transporter EAAC1**. *J Biol Chem* 2016, **291**:11852–11864.
24. Grewer C, Balani P, Weidenfeller C, Bartusel T, Tao Z, Rauen T: **Individual subunits of the glutamate transporter EAAC1 homotrimer function independently of each other**. *Biochemistry* 2005, doi:10.1021/bi050987n.
25. Leary GP, Stone EF, Holley DC, Kavanaugh MP: **The glutamate and chloride permeation pathways are colocalized in individual neuronal glutamate transporter subunits**. *J Neurosci* 2007, doi:10.1523/JNEUROSCI.4851-06.2007.
26. Koch HP, Brown RL, Larsson HP: **The glutamate-activated anion conductance in excitatory amino acid transporters is gated independently by the individual subunits**. *J Neurosci* 2007, doi:10.1523/JNEUROSCI.0118-07.2007.
27. Akyuz N, Altman RB, Blanchard SC, Boudker O: **Transport dynamics in a glutamate transporter homologue**. *Nature* 2013, **502**:114–118.
28. Stolzenberg S, Khelashvili G, Weinstein H: **Structural intermediates in a model of the substrate translocation path of the bacterial glutamate transporter homologue Glt_{Ph}**. *J Phys Chem B* 2012, **116**:5372–5383.
29. Jiang J, Shrivastava IH, Watts SD, Bahar I, Amara SG: **Large collective motions regulate the functional properties of glutamate transporter trimers**. *Proc Natl Acad Sci U S A* 2011, doi:10.1073/pnas.1112216108.
30. Groeneveld M, Slotboom DJ: **Rigidity of the Subunit Interfaces of the Trimeric Glutamate Transporter GltT During Translocation**. *J Mol Biol* 2007, **372**:565–570.
31. Verdon G, Boudker O: **Crystal structure of an asymmetric trimer of a bacterial glutamate transporter homolog**. *Nat Struct Mol Biol* 2012, doi:10.1038/nsmb.2233.
32. Groeneveld M, Slotboom DJ: **Na^+:Aspartate coupling stoichiometry in the glutamate transporter homologue Glt_{Ph}**. *Biochemistry* 2010, **49**:3511–3513.
33. Ewers D, Becher T, Machtens JP, Weyand I, Fahlke C: **Induced fit substrate binding to an archeal glutamate transporter homologue**. *Proc Natl Acad Sci U S A* 2013, **110**:12486–12491.
34. Alleva C, Kovalev K, Astashkin R, Bernd MI, Baeken C, Balandin T, Gordeliy V, Fahlke C, MacHtens JP: **Na^+-dependent gate dynamics and electrostatic attraction ensure substrate coupling in glutamate transporters**. *Sci Adv* 2020, **6**:eaba9854.
35. Reyes N, Oh S, Boudker O: **Binding thermodynamics of a glutamate transporter homolog**. *Nat Struct Mol Biol* 2013, **20**:634–640.
36. Oh S, Boudker O: **Kinetic mechanism of coupled binding in sodium-aspartate symporter Glt_{Ph}**. *Elife* 2018, **7**:1–20.
37. Hänelt I, Jensen S, Wunnicke D, Slotboom DJ: **Low affinity and slow Na^+ binding precedes high affinity aspartate binding in the secondary-active transporter Glt_{Ph}**. *J Biol Chem* 2015, **290**:15962–15972.
38. Segel IH: **Enzyme Kinetics**. In *Encyclopedia of Biological Chemistry: Second Edition*. . 2013.
39. Zimmermann I, Egloff P, Hutter CAJ, Arnold FM, Stohler P, Bocquet N, Hug MN, Huber S, Siegrist M, Hetemann L, et al.: **Synthetic single domain antibodies for the conformational trapping of membrane proteins**. *Elife* 2018, doi:10.7554/eLife.34317.
40. Lolkema JS, Slotboom DJ: **Models to determine the kinetic mechanisms of ioncoupled transporters**. *J Gen Physiol* 2019, **151**:369–380.
41. King EL, Altman C: **A schematic method of deriving the rate laws for enzyme-catalyzed reactions**. *J Phys Chem* 1956, doi:10.1021/j150544a010.
42. Zimmermann I, Egloff P, Hutter CAJ, Kuhn BT, Bräuer P, Newstead S, Dawson RJP, Geertsma ER, Seeger MA: **Generation of synthetic nanobodies against delicate proteins**. *Nat Protoc* 2020, doi:10.1038/s41596-020-0304-x.

43. Ryan RM, Kortt NC, Sirivanta T, Vandenberg RJ: **The position of an arginine residue influences substrate affinity and K^+ coupling in the human glutamate transporter, EAAT1**. *J Neurochem* 2010, doi:10.1111/j.1471-4159.2010.06796.x.
44. Verdon G, Oh SC, Serio R, Boudker O: **Coupled ion binding and structural transitions along the transport cycle of glutamate transporters**. *Elife* 2014, **2014**:1–23.
45. Ciftci D, Ciftci D, Huysmans GHM, Wang X, He C, Terry D, Zhou Z, Fitzgerald G, Blanchard SC, Blanchard SC, et al.: **Single-molecule transport kinetics of a glutamate transporter homolog shows static disorder**. *Sci Adv* 2020, doi:10.1126/sciadv.aaz1949.
46. Garaeva AA, Guskov A, Slotboom DJ, Paulino C: **A one-gate elevator mechanism for the human neutral amino acid transporter ASCT2**. *Nat Commun* 2019, doi:10.1038/s41467-019-11363-x.
47. Garaeva AA, Slotboom DJ: **Elevator-type mechanisms of membrane transport**. *Biochem Soc Trans* 2020, **48**:1227–1241.
48. Zhang Z, Tao Z, Gameiro A, Barcelona S, Braams S, Rauen T, Grewer C: **Transport direction determines the kinetics of substrate transport by the glutamate transporter EAAC1**. *Proc Natl Acad Sci U S A* 2007, **104**:18025–18030.
49. Punjani A, Rubinstein JL, Fleet DJ, Brubaker MA: **CryoSPARC: Algorithms for rapid unsupervised cryo-EM structure determination**. *Nat Methods* 2017, doi:10.1038/nmeth.4169.
50. Terwilliger TC, Sobolev O V., Afonine P V., Adams PD: **Automated map sharpening by maximization of detail and connectivity**. *Acta Crystallogr Sect D Struct Biol* 2018, doi:10.1107/S2059798318004655.
51. Emsley P, Lohkamp B, Scott WG, Cowtan K: **Features and development of Coot**. *Acta Crystallogr Sect D Biol Crystallogr* 2010, doi:10.1107/S0907444910007493.
52. Afonine P V., Poon BK, Read RJ, Sobolev O V., Terwilliger TC, Urzhumtsev A, Adams PD: **Real-space refinement in PHENIX for cryo-EM and crystallography**. *Acta Crystallogr Sect D Struct Biol* 2018, doi:10.1107/S2059798318006551.
53. Pettersen EF, Goddard TD, Huang CC, Couch GS, Greenblatt DM, Meng EC, Ferrin TE: **UCSF Chimera - A visualization system for exploratory research and analysis**. *J Comput Chem* 2004, doi:10.1002/jcc.20084.